Monatshefte für Chemie - Chemical Monthly (2021) 152:137–149
https://doi.org/10.1007/s00706-020-02716-0

ORIGINAL PAPER

# Development of new hetero-steroid hybrids with antiproliferative activity against MCF-7 breast cancer cells

**Muhamad Mustafa[1] · Ahmed El-Kardocy[2] · Yaser A Mostafa[3]**

Received: 9 July 2020 / Accepted: 19 November 2020 / Published online: 8 January 2021


## Abstract

In continuation of our efforts to develop new antiproliferative agents that could be effective and selective in treatment of cancer, we designed and synthesized new hybrid structures containing an arylsulfonamide scaffold linked to a steroidal skeleton through a 1,2,3-triazole ring. Both in vitro cytotoxicity on breast MCF-7 cancer cells and human placental aromatase enzyme (pAROM) inhibition assays were performed on new hybrids. All new hybrids showed marked cytotoxic activity against breast MCF-7 cancer cells ($IC_{50}$ = 3.56–43.76 μM) in comparison to staurosporine ($IC_{50}$ = 4.06 μM). Tumor selectivity index was higher for some of the new hybrids on normal fibroblast (F-180) cells (TS = 1.5–25) in comparison to staurosporine (TS = 2.5). The *p*-nitro derivative exhibited the best inhibitory activity on the pAROM with an $IC_{50}$ of 64.6 ng/$cm^3$, compared to hybrids unsubstituted derivative, *p*-bromo derivative, and letrozole ($IC_{50}$ = 375.14, 269.86, and 132.86 ng/$cm^3$, respectively). Furthermore, the *p*-nitro hybrid arrested the cell cycle selectively at the G2/M phase, in addition to inducing both early and late apoptotic processes of breast MCF-7 cancer cells. Molecular docking studies were performed within pAROM to explore the binding modes of the new hybrids. Collectively, the antiproliferative profile of new hybrids indicates how good they are as promising leads for developing tumor-specific cytotoxins, and deserve further studies to optimize their structure and in vivo activity.

### Graphic abstract

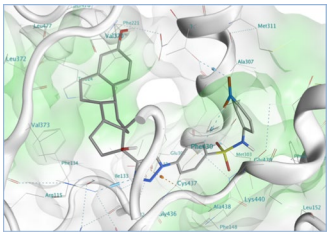

**Keywords** Aromatase inhibitors · Steroidal hybrids · Anti-tumor agents · Flow cytometry · Molecular docking

**Electronic supplementary material** The online version of this article (https://doi.org/10.1007/s00706-020-02716-0) contains supplementary material, which is available to authorized users.

✉ Yaser A Mostafa
y3abdelh@uwaterloo.ca

[1] Medicinal Chemistry Department, Faculty of Pharmacy, Deraya University, Minia 61111, Egypt

[2] Faculty of Pharmacy, Student Research Center, Assiut University, Assiut 71526, Egypt

[3] Pharmaceutical Organic Chemistry Department, Faculty of Pharmacy, Assiut University, Assiut 71526, Egypt

## Introduction

Cancer is still globally a major health problem that affected a large number of people around the world [1–3]. Its high morbidity and mortality rates come next after cardiac disease [4]. The pivotal role of the aromatase enzyme in the aromatization of androgens to estrogens, and the correlation of the high level of estrogens with stimulation of the progression and metastasis of hormone-dependent breast cancer (HDBC) in both pre- and post-menopausal women, targeted the use of the apoptogenic activity of the aromatase inhibitors (AIs)

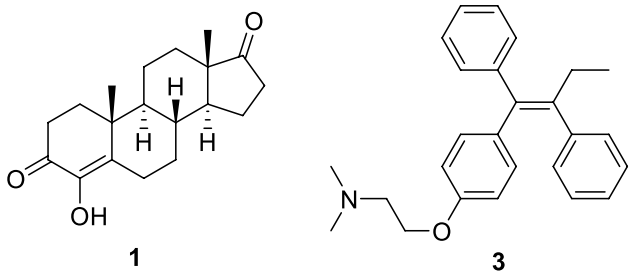


**Fig. 1** Chemical structures of tamoxifen and 4-adione

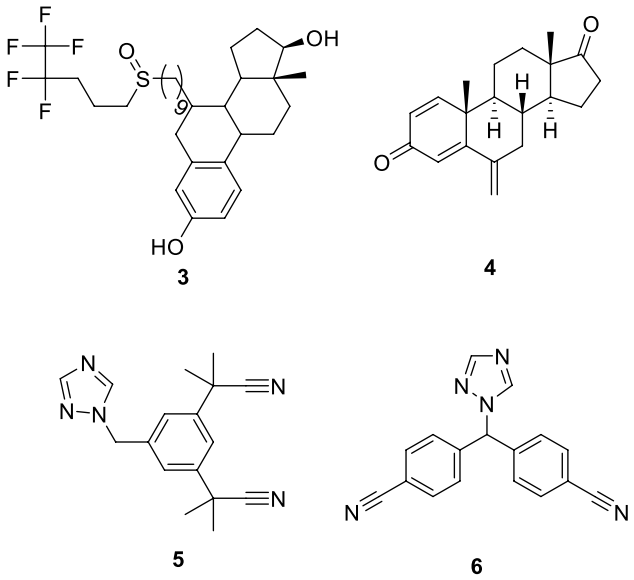


**Fig. 2** Chemical structures of steroidal and non-steroidal AIs

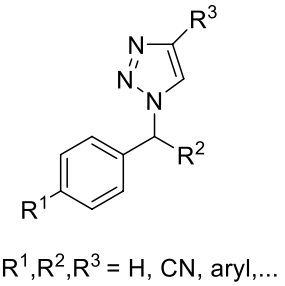


**Fig. 3** Triazole AIs **7**, designed by Touaibia group

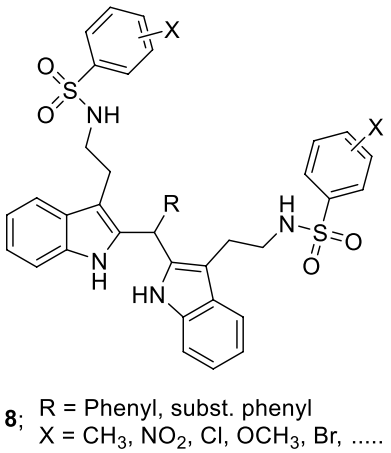


**Fig. 4** Pingaew indole AIs **8**, bearing sulfonamide scaffold

a useful strategy in the treatment of HDBC [5–7]. Interestingly, the selective inhibition of the aromatase enzyme does not interfere with the other steroids biosynthesis and generally well-tolerated with minimal side effects on uterus [8, 9]. 4-Hydroxyandrostenedione (4-adione, **1**) was found to be one of the most potent AIs with higher efficacy and fewer side effects than other remedies previously used for the treatment of HDBC such as tamoxifen (**2**) [10] (Fig. 1).

Steroidal (type I) AIs such as fulvestrant (**3**), exemestane (**4**); and non-steroidal (type II) AIs like anastrazole (**5**) and letrozole (**6**); that clinically used and approved by the US Food and Drug Administration (FDA) for treatment of HDBC in post-menopausal women [11] (Fig. 2).

Discovery of novel cytotoxic agents using naturally bioactive compounds as a building block is one of the attractive avenue in drug development these days. Moreover, designed multiple ligands (DML) have proved their effectiveness as an attractive alternative for either combination therapies or single target ligands [12]. DMLs widely used now to eliminate resistance developed by cancerous tissue to drug therapy, also to decrease to large extent the risk of drug-drug interactions and improve patient compliance by reduction of medications' number [13, 14]. Conjugates as a class of DMLs are designed to have their molecular scaffolds of each biological target separated by a distinct linker group [15, 16]. Dual aromatase-sulfatase inhibitors (DASIs) are a widespread class of conjugates which targeting estrogen receptors (ERs) [17]. Anastrazole (**5**) and letrozole (**6**) are DASIs that clinically used as drugs for the treatment of HDBC [17]. Triazoles are well-known pharmacophores in a diverse range of biologically-active molecules because of their potential biomolecular characteristics such as the capability of H-bond formation and metabolic stability [18, 19]. Touaibia group reported an equipotent set of 1,4-disubstituted-1,2,3-triazoles **7**, designed-based on letrozole and anastrazole antiproliferative profile [20] (Fig. 3).

Pingaew et al. reported 34 new indoles **8**, bearing sulfonamide moiety to explore the crucial structural features that should be fulfilled in building AIs (such as triazole N-atom, sulfonamide moiety, $–NO_2$ group, hydrophobicity, H-bonding, etc.) and required for interaction with various amino acid residues within aromatase enzyme active site [21–23] (Fig. 4).

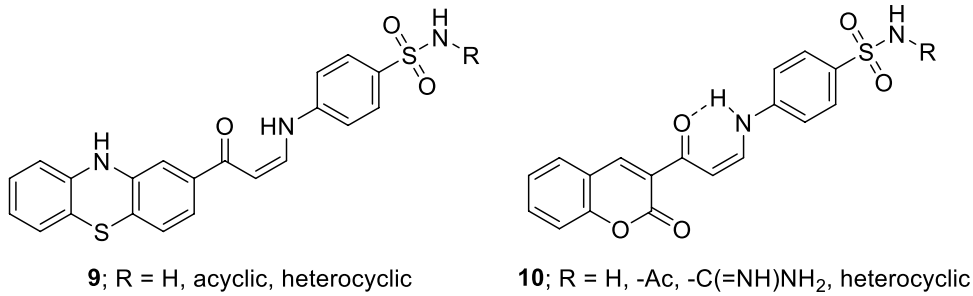


**Fig. 5** Ghorab non-steroidal sulfonamide AIs

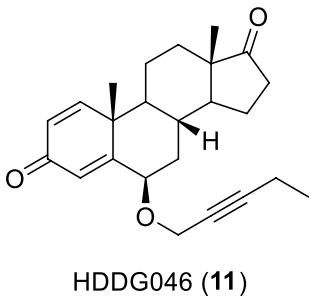


**Fig. 6** Steroidal inhibitor of pAROM (HDDG046, **11**) built by Ghosh

On the same avenue and based on Pingaew findings, Ghorab et al. developed potent and selective aromatase inhibitors, compounds **9** and **10**, with apoptosis induction capability [24] (Fig. 5). In addition, Ghorab performed molecular docking studies within aromatase active site to explore the H-bonding and hydrophobic interactions between the sulfonyl group oxygen and aromatic skeleton with Met 374, Cys 437, Ala 306, and Ala 307 and their correlation with inhibition of aromatase catalytic activity [25].

Moreover, Ghosh et al. succeed to co-crystalize the human placental aromatase enzyme (CYP19) with a highly potent inhibitor, compound **11** (HDDG046), after using the step-by-step chemical modification of both 4-adione and exemestane skeletons as the main building block for building such potent inhibitor [26] (Fig. 6).

From all these interesting findings, we think likely to design new conjugate in which the non-steroidal part of recently reported pAROM inhibitors by Ghorab, Touaibia, and Ghosh replaced by the steroidal ring of 17β-estradiol (E2), while preserving both the sulfonamide and 1,2,3-triazole moieties, could be a promising avenue to develop potent human pAROM inhibitors which capable of fitting better within pAROM active site and accommodate its large hydrophobic pocket, as shown in Fig. 7.

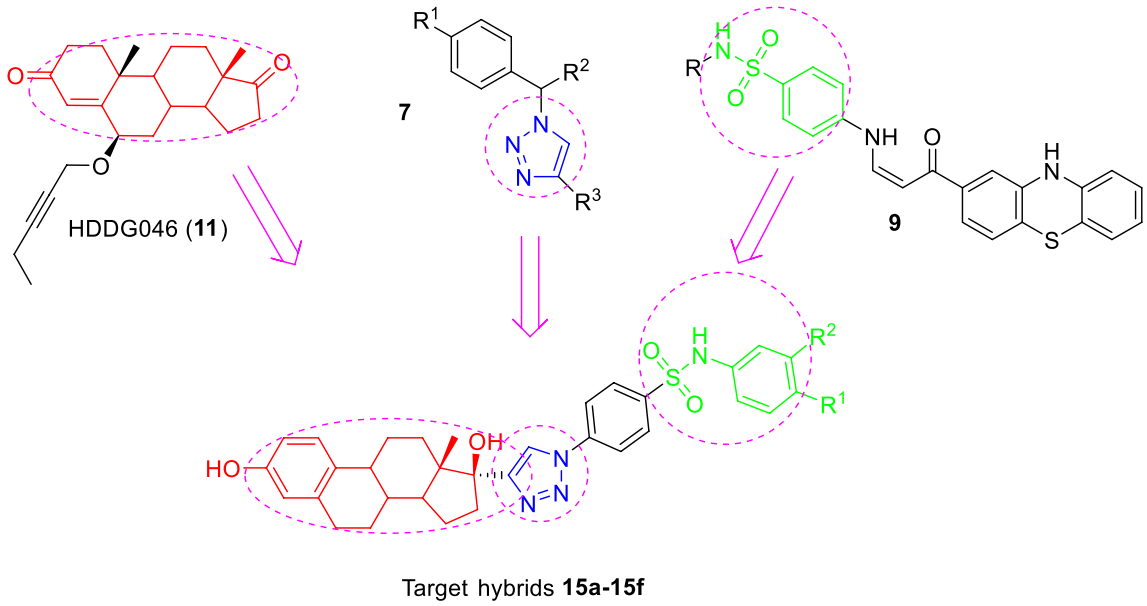


**Fig. 7** Design of the target hybrids **15a**–**15f** from literature cytotoxic scaffolds

## Results and discussion

The intermediates and target hybrids were prepared according to the sequence of reactions shown in Scheme 1. Intermediate **13**, the azidobenzenesulfonyl chloride, was prepared from sulfanilic acid (**12**) according to reported methods used for the preparation of various azides and sulfonyl chlorides of different sulfonic acids [27, 28]. On the other hand, one of the intermediates (intermediate **14a**) was reported in 2011 by Mirian et al. [29], while the other five intermediates **14b**–**14f** were reported by our group [30]. The target 1,2,3-triazole sulfonamides **15a**–**15f** were prepared in high yields via Cu(I)-catalyzed azide-alkyne cycloaddition (CuAAC) reaction using the catalytic $CuSO_4$/Na ascorbate mixture in THF/$H_2O$ mixture. Spectral characterization of hybrids **15a**–**15f** was done using both $^1$H and $^{13}$C NMR, while their purity was assessed via C,H,N elemental analyses and results were within an acceptable range of ± 0.4. The $^1$H NMR spectra of the prepared cycloadducts **15a**–**15f** showed the characteristic broad singlet signal of the sulfonamide group above $\delta = 10.00$ ppm (except with nitro derivatives **15d** and **15f** it appeared above 11.00 ppm), also, all the new hybrids **15a**–**15f** showed a common singlet signal at 8.61–8.66 ppm corresponding to the –CH of the newly formed 1,2,3-triazole ring. Moreover, $^{13}$C NMR spectra of all the new hybrids were fundamentally distinguishable according to various anilines used.

## In vitro cytotoxic activity

Hybrids **15a**–**15f** were tested for their cytotoxicity on breast cancer MCF-7 cells. Being a matter of concentration dependence, the percentages of cell viability declined significantly upon increasing the concentration of the new hybrids **15a**–**15f** as shown in Table 1 (as shown in dose–response curves in supporting information).

All the new hybrids **15a**–**15f** suppressed MCF-7 cells viability by a percentage exceeds 50% at 100 μM concentration. The MTT assay results demonstrated that hybrid **15d** which carries a nitro group at para position possessed the best inhibitory activity on MCF-7 cells with an $IC_{50}$ value of 3.57 μM compared to the reference drug staurosporine [staurosporine (STS) was used as a clinically broad-spectrum cytotoxic drug that has shown effectiveness in in vitro models of various tumors such as colon, leukemia, and breast cancer; $IC_{50} = 4.06$ μM], as shown in Table 1.

Hybrids **15a** and **15b** showed equipotency to each other ($IC_{50}$ values of 11.02 and 11.20 μM, respectively) which is weaker then hybrid **15d** and reference drug bust still in the low micromolar range. Moreover, hybrids **15c**, **15e**, and **15f** showed weaker inhibitory activity on MCF-7 than all other hybrids and reference drug ($IC_{50} = 37.9$, 22.4, and 43.7 μM, respectively). The obtained results revealed that the cytotoxic activity was relatively decreased with *p*-Br and *p*-$OCH_3$ groups (hybrids **15c** and **15e**, respectively). Interestingly, incorporation of a $NO_2$ group as with hybrid **15d** boosted the cytotoxic activity significantly, although,

**Scheme 1**

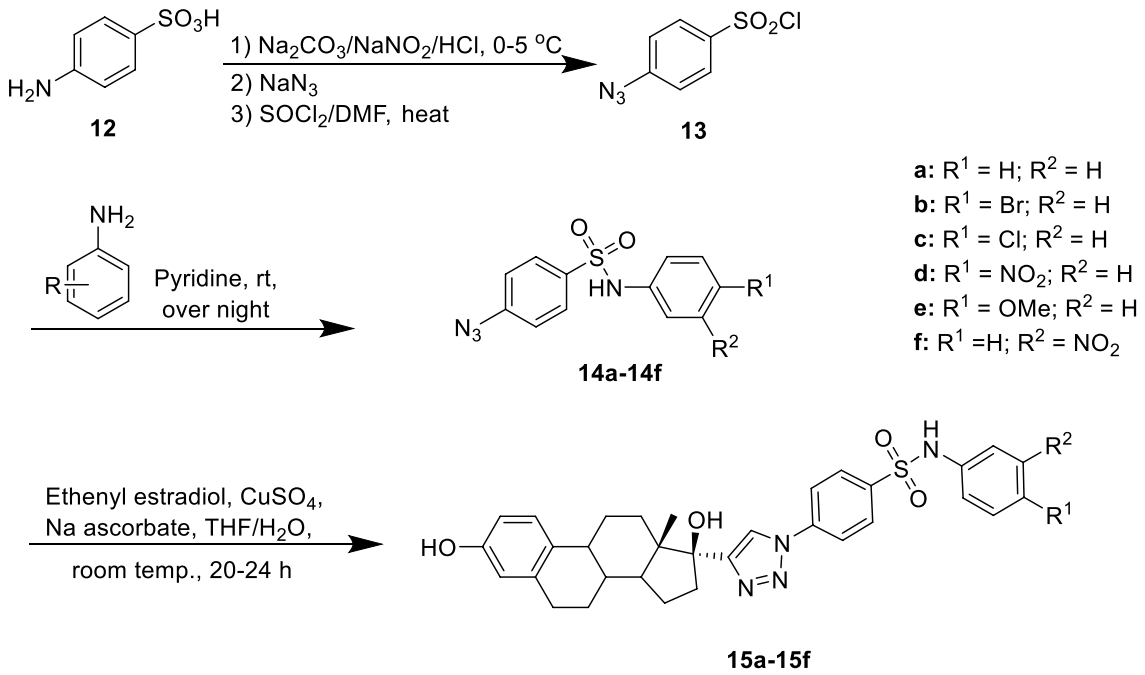

**Table 1** Dose-dependent inhibition of breast MCF-7 cancer cells via hybrids **15a**–**15f**

| Compound | % Viability[a] | | | | |
|---|---|---|---|---|---|
| | 100 μM | 25 μM | 6.25 μM | 1.56 μM | 0.39 μM |
| Ref.[b] | 28.48 ± 0.007 | 35.92 ± 0.005 | 47.51 ± 0.006 | 56.21 ± 0.008 | 66.85 ± 0.004 |
| **15a** | 34.22 ± 0.003 | 39.82 ± 0.005 | 54.30 ± 0.008 | 68.23 ± 0.005 | 76.63 ± 0.005 |
| **15b** | 33.24 ± 0.011 | 44.87 ± 0.004 | 53.12 ± 0.008 | 65.11 ± 0.008 | 75.88 ± 0.005 |
| **15c** | 41.21 ± 0.008 | 54.79 ± 0.005 | 62.63 ± 0.008 | 76.77 ± 0.006 | 82.15 ± 0.007 |
| **15d** | 28.63 ± 0.012 | 36.27 ± 0.004 | 45.45 ± 0.005 | 53.65 ± 0.004 | 66.99 ± 0.011 |
| **15e** | 39.19 ± 0.007 | 50.73 ± 0.004 | 58.23 ± 0.002 | 67.27 ± 0.005 | 78.04 ± 0.009 |
| **15f** | 45.01 ± 0.005 | 54.27 ± 0.004 | 61.09 ± 0.005 | 71.50 ± 0.004 | 81.62 ± 0.004 |

[a]Data were reported on MCF-7 cells as mean ± SD ($n = 3$)

[b]Staurosporine was used as a positive control in the cytotoxicity screening

**Table 2** $IC_{50}$ of new hybrids **15a**–**15f** on MCF-7 and F-180 cells

| Compound | $IC_{50}$/μM[a] | | SI |
|---|---|---|---|
| | MCF-7[b] (column A) | F-180[c] (column B) | |
| Ref.[d] | 4.1 ± 0.13 | 10.2 ± 0.41 | 2.5 |
| **15a** | 11.0 ± 0.36 | 34.1 ± 0.08 | 3 |
| **15b** | 11.2 ± 0.36 | 66.2 ± 0.18 | 6 |
| **15c** | 37.9 ± 1.24 | 80.6 ± 0.54 | 2 |
| **15d** | 3.6 ± 0.11 | 89.3 ± 0.33 | 25 |
| **15e** | 22.4 ± 0.73 | 100.8 ± 0.14 | 4.5 |
| **15f** | 43.8 ± 1.43 | 63.1 ± 0.26 | 1.5 |

[a]Concentration of test compounds in micromolar which inhibited 50% of cells growth

[b]MCF-7 breast cancer cells

[c]Normal fibroblast cells

[d]Staurosporine was used as a positive control in $IC_{50}$ determination

**Table 3** $IC_{50}$ data of hybrids **15a**–**15f** using CYP19 screening assay

| Compound | % of inhibition[a] | | | | $IC_{50}$/ng/cm$^{3}$[a] |
|---|---|---|---|---|---|
| | 10[b] | 1 | 0.1 | 0.01 | |
| Ref.[c] | 90.73 | 82.09 | 41.51 | 22.57 | 0.13 |
| **15a** | 81.08 | 69.79 | 31.21 | 10.50 | 0.37 |
| **15b** | 82.78 | 63.75 | 36.99 | 22.22 | 0.27 |
| **15c** | –[d] | – | – | – | – |
| **15d** | 91.14 | 77.90 | 58.92 | 28.84 | 0.06 |
| **15e** | – | – | – | – | – |
| **15f** | – | – | – | – | – |

[a]Errors are within ± 2%

[b]Log concentration used

[c]Letrozole was used as a positive control in the human placental aromatase (CYP19) screening assay

[d]Not tested

changing the position of such $NO_2$ group to the meta-position decreased the inhibitory activity significantly as seen with hybrid **15f**.

## In vitro cytotoxic activity towards normal fibroblast (F-180) cells

In an attempt to investigate the selectivity of the target compounds on cancer cells, an in vitro cytotoxic assay was performed on the noncancerous normal fibroblast cell lines (F-180). The obtained $IC_{50}$s showed that all the synthesized hybrids **15a**–**15f** were substantially tumor-specific cytotoxins than the reference drug, as shown in Table 2. Tumor selectivity (TS) was calculated by dividing the mean $IC_{50}$ values against normal fibroblast cells (F-180) by the mean $IC_{50}$ against breast MCF-7 cancer cells (TS = column B/column A), Table 2. Upon comparing the calculated TS values, compound **15d** showed the highest selectivity towards MCF-7 cells among the test hybrids even more the reference drug, staurosporine. Moreover, hybrids **15a**, **15b**, and **15e** showed better tumor selectivity than STS. On the other hand, hybrids **15c** and **15f** were found to be slightly less selective cytotoxic agents than staurosporine against breast MCF-7 cancer cells.

## Inhibition of aromatase enzyme

Based on various literature studies, inhibition of human placental aromatase enzyme (CYP19) is one of the fundamental approaches in treating HDBCs [31, 32]. Hence, the most potent hybrids **15a**, **15b**, and **15d** were evaluated for their ability to inhibit aromatase enzyme against the well-known aromatase inhibitor letrozole (Table 3). All the test hybrids showed a remarkable ability to inhibit the aromatase enzyme (a dose-dependent inhibition). Hybrid **15d** has the highest ability to inhibit CYP19 enzyme embedded in MCF-7 cells with an $IC_{50}$ of 64.6 ng/cm$^3$, which is almost 1.5 times the potency of letrozole ($IC_{50}$ = 132.8 ng/cm$^3$). Hybrids **15a** and **15b** showed comparable inhibition potency about half that of letrozole.

**Table 4** Cell cycle distribution induced by hybrid **15d**

| Compound | Cell cycle phases | | | |
|---|---|---|---|---|
| | G0-G1 | S | G2/M | Pre-G1 (sub-G1) |
| **15d** | 53.26 | 36.06 | 10.68 | 1.76 |
| Control | 32.94 | 31.42 | 35.64 | 18.43 |

## Cell cycle analysis by flow cytometry

Regularly, antitumor agents abort the proliferation and the growth of cancerous cells by arresting cell division at different checkpoints [33]. Treating cancer cells with potent antitumor agents disengages the distinguish cells in different phases of the cell cycle. In the current research, MCF-7 cells were treated with the most potent sulfonamide **15d** at its $IC_{50}$ value. The obtained data (as shown in Table 4) indicated that hybrid **15d** substantially arrested the G2/M phase compared to the negative control (35.64% and 10.68%, respectively) (Fig. 8).

## Induction of cellular apoptosis

Hybrid **15d** showed a remarkable ability to induce apoptosis in MCF-7 cell lines, after staining with annexin V-FITC and propidium iodide. At its $IC_{50}$ concentration, hybrid **15d** initiated cellular apoptosis and dispersed cellular integrity, as shown in Fig. 9. The percentage of early apoptotic cells (the lower right quadrant) increased to declare 4.42% while the negative control was 0.88%. Regarding cellular integrity dispersion, **15d** elevated the late apoptotic cells (the upper right quadrant) up to 11.99% compared to only 0.51% for

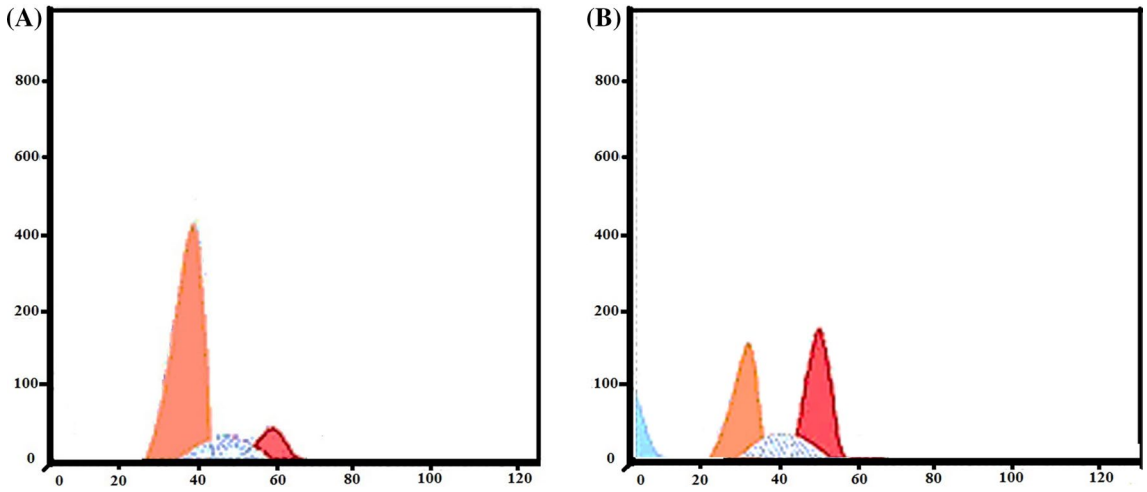


**Fig. 8** Cell cycle analysis of MCF-7 cells treated with PI at test $IC_{50}$s; **a** untreated (control) cells, **b** cells treated with hybrid **15d**

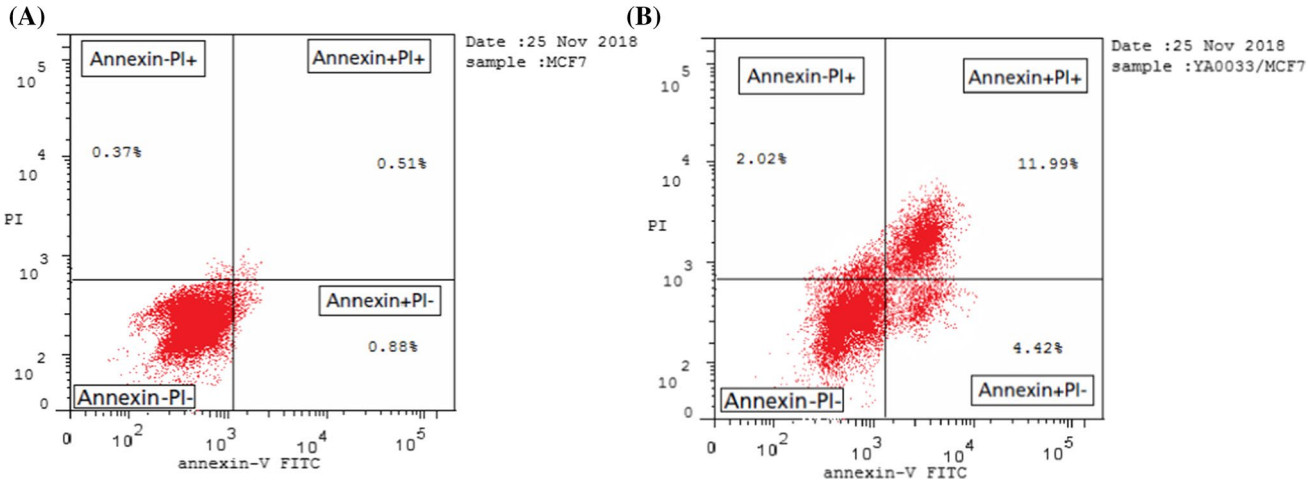


**Fig. 9** Contour diagram of Annexin V/PI flow cytometry: **a** untreated cells, **b** cells treated with hybrid **15d** (lower left: live cells; lower right: early apoptotic cells; upper right: late apoptotic cells; upper left: necrotic cells)

the untreated cells. Necrosis was boosted to a lesser extent (2.02%) compared to negative control = 0.37% on MCF-7 cells. Subsequently, hybrid **15d** performed most of its activity through induction of apoptosis.

## Molecular modelling studies

To study the possible binding modes of these new sulfonamides within the human placental aromatase (CYP19; pAROM), molecular modelling studies were performed using X-ray crystal structure data for aromatase obtained from the protein data bank (PDB: ID 5JL9) [34] using previously co-crystallized ligands such as androstenedione (AE), exemestane, and HDDG046 as reference compounds.

All the intermolecular interaction energies (S in kJ/mol) and amino acid residues with various functional groups of new hybrids were summarized in Table 5. From the docking data, all the docked hybrids **15a**–**15f** successfully occupied the active site with good energy scores ranging from − 17.7 to − 28.8 kJ/mol compared to − 24.3, − 23.5, and − 31 kJ/mol observed for AE, exemestane, and HDDG046, respectively.

The binding interactions of new hybrids **15a**–**15f** with amino acid residues were found to be either through hydrogen bonding or π–H interactions. It noteworthy that most of the hydrogen bonding occurred through S=O functional

**Table 5** Molecular modeling data for the target hybrids **15a**–**15f**, AE, exemestane, and HDDG046 in pAROM (PDB: ID 5JL9)

| Compound | S[i] | H-bonding | | Other interactions | |
|---|---|---|---|---|---|
| | | (A)[a] | (B)[b] | (C)[c] | (D)[d] |
| AE | − 24.3 | Ala 306[e]<br>Arg 115[e]<br>Met 374[e] | C=O (3.31)<br>C=O (3.37)<br>C=O (2.82) | – | – |
| Exemestane | − 23.5 | Ala 306[e]<br>Arg 115[e]<br>Met 374[e] | C=O (3.13)<br>C=O (3.32)<br>C=O (2.71) | – | – |
| HDDG046 | − 31 | Leu 372[f]<br>Ala 306[e]<br>Arg 115[e]<br>Met 374[e] | C16 (3.29)<br>C=O (3.09)<br>C=O (3.39)<br>C=O (2.91) | Phe 221[g] | $C_{24}$ (3.93) |
| **15a** | − 28.2 | Met 303[f]<br>Ala 306[e]<br>Cys 437[f] | S=O (3.85)<br>S=O (4.04)<br>$C_{17}$–OH (3.20) | Thr 310[h] | Triazole ring (3.89) |
| **15b** | − 26.6 | Met 374[f]<br>Ala 307[e] | Ph–OH (3.26)<br>S=O (3.16) | Thr 310[h] | Triazole ring (3.99) |
| **15c** | − 17.7 | Met 303[f]<br>Ser 199[e]<br>Ala 307[e] | NH (3.62)<br>S=O (3.09)<br>S=O (3.35) | – | – |
| **15d** | − 28.8 | Met 311[f]<br>Cys 437[f]<br>Met 303[f]<br>Arg 115[e]<br>Thr 310[e] | $N^+$=O (3.50)<br>$N^+$–$O^-$ (3.53)<br>S=O (2.78/3.38)<br>Triazole-N-(2.98)<br>$N^+$–$O^-$ (3.09) | Cys 437[h] | Triazole ring (3.56) |
| **15e** | − 22 | Met 303[f]<br>Ala 307[e]<br>Ser 199[e] | NH (3.52)<br>S=O (3.34)<br>S=O (3.15) | – | – |
| **15f** | − 21.8 | Cys 437[e]<br>Ala 307[e]<br>Ala 438[e] | $C_{17}$–OH (3.22)<br>S=O (3.36)<br>$C_{17}$–OH (3.19) | Val 370[h] | Phenolic ring (3.79) |

[a]H-bond forming residues and types

[b]Function group forming H-bond and bond length (Å)

[c]Other interactions residues and types

[d]Function group of interaction and bond length (Å)

[e]Hydrogen acceptor

[f]Hydrogen donor

[g]H–π

[h]π–H

[i]Energy score (δ kJ/mol)

group compared to its bioisostere (C=O) in the other reported co-crystallized ligands (AE, exemestane, and HDDG046), indicating the success of this bioisosteric replacement in the design of these new hybrids. Hybrid **15d** showed additional H-bond interactions with Met 311, Cys 437, and Thr 310 residues through its *p*-$NO_2$ group, which helped in anchoring the whole molecule efficiently within the pAROM active site (Fig. 10), explaining its bitter interaction energy compared to both AE and exemestane reference compounds. Moreover, all the three reference compounds shared a common H-bond interaction with Arg 115, which was found also with the most potent hybrid **15d** confirming its superior potency over its congers as an inhibitor of the pAROM. Interestingly, changing the position of the nitro group from *para*-position (as with hybrid **15d**) to the *meta*-position (as with hybrid **15f**) leads to a remarkable decrease in the binding energy score of hybrid **15f** with pAROM. Additionally, the π–H interaction with the active site amino acid residues was found mainly through the triazole ring N-atom of compounds **15a**, **15b**, and **15d**, and to lesser extent with a phenolic ring as with compound **15f**, while compounds **15c** and **15e** failed to show such interaction, as shown in Table 5.

## Conclusion

To summarize, a series of novel human placental aromatase inhibitors containing a hybrid of the steroidal skeleton, 1,2,3-triazole ring, and a benzenesulfonamide scaffold were synthesized. The new hybrids showed a remarkable selective inhibition for MCF-7 breast cancer cells compared to non-cancerous fibroblast F-180 cells. Hybrid **15d** was profoundly tumor-specific cytotoxin compared to staurosporine and letrozole on MCF-7 cells and aromatase enzyme, respectively. Additionally, its ability to abort the proliferation and the growth of MCF-7 breast cancer cells at the G2/M phase of the cell cycle with apoptosis induction mechanism. The new hybrids **15a**–**15f** complete occupied the pAROM active site during molecular docking studies. Obviously, the steroidal skeleton gave the extra fitting of the target molecules within aromatase active site causing such strong inhibition profile. Within the new hybrids, hybrids **15a**, **15b**, and **15d** could be considered as promising anti-proliferative aromatase inhibitors for the treatment of HDBC and deserves further in vivo studies.

## Experimental

All solvents and reagents were of pure grades from Fluka®, Sigma-Aldrich®, or Alfa-Aesar® and used without further purification; ethinyl estradiol (EE) was obtained from Carbosynth® chemical company. Purification of various intermediates and final hybrids was performed by flash chromatography using Silicycle® silica gel and a mixture of EtOAc/hexane as an eluent. NMR spectra were recorded on a JEOL ECA-500 II Spectrometer using DMSO-$d_6$ (Faculty of Science, Almansura University, Almansura, Egypt), as a solvent, and chemical shifts ($\delta$) for $^1$H NMR spectra were recorded relative to TMS ($Me_4Si$; $\delta = 0.00$ ppm) as an internal standard, while $^{13}$C NMR spectra were recorded relative to DMSO-$d_6$ ($\delta = 39.5$ ppm, central peak) residual peak and coupling constants ($J$) in Hertz (Hz). High-resolution mass spectra (HRMS, electrospray ionization ESI) were obtained on JEOL HX110 double-focusing mass spectrometer, and elemental analyses (C, H, N) were measured on Vario El-Elementar CHN Elemental Analyzer (Al Azahr University, New City, and Cairo, Egypt) for all final hybrids and were found within ± 0.4 of their calculated values. Finally, melting points were determined on electrothermal melting point apparatus (SMP1, UK).

### Synthesis of 4-azidobenzenesulfonyl chloride (13)

To 25 g sulfanilic acid (**12**, 1.44 mol) in 20 $cm^3$ $H_2O$, 0.58 g sodium carbonate ($5.47 \times 10^{-3}$ mol) was added portion-wise with continuous and vigorous stirring. After effervescence subside, 0.84 g sodium nitrite ($12.17 \times 10^{-3}$ mol) was added and stirring was continued till complete dissolution, followed by a diazotization step using 1.4 $cm^3$ conc. HCl diluted with 3 $cm^3$ $H_2O$ at 0–5 °C. A white precipitate was formed, which was filtered under vacuum, and finally washed with 8 $cm^3$ cold water to afford the diazotized sulfanilic acid. To a suspension of the former white precipitate (was used in the next step without further purification) in 10 $cm^3$ $H_2O$, was added as an aqueous saturated solution of sodium azide (8 g in 20 $cm^3$ $H_2O$) portion-wise with vigorous stirring till nitrogen gas evolution ceased. Sodium chloride was added to salt-out the formed azido derivative of sulfanilic acid as a white precipitate, which was filtered under vacuum, washed with cold water, and finally dried under vacuum for the next step affording 20 g (70.7%). M.p.: > 200 °C [28]. The dried azido-derivative of sulfanilic acid was dissolved with stirring in a mixture of 3 $cm^3$ thionyl chloride/1 drop of DMF, and heated for half an hour till boiling, after that, the remaining thionyl chloride was removed under vacuum and the remaining residue was extracted with dry ether ($2 \times 5$ $cm^3$). The etherial extract was concentrated under vacuum to afford compound **13** as yellowish-white solid 15.9 g (73%). M.p.: 59–61 °C [27].

### General procedure for preparation of compounds 14a–14f

In 1 $cm^3$ dry pyridine, equimolar amounts of **13** and substituted aniline ($1 \times 10^{-5}$ mol) was mixed with stirring.

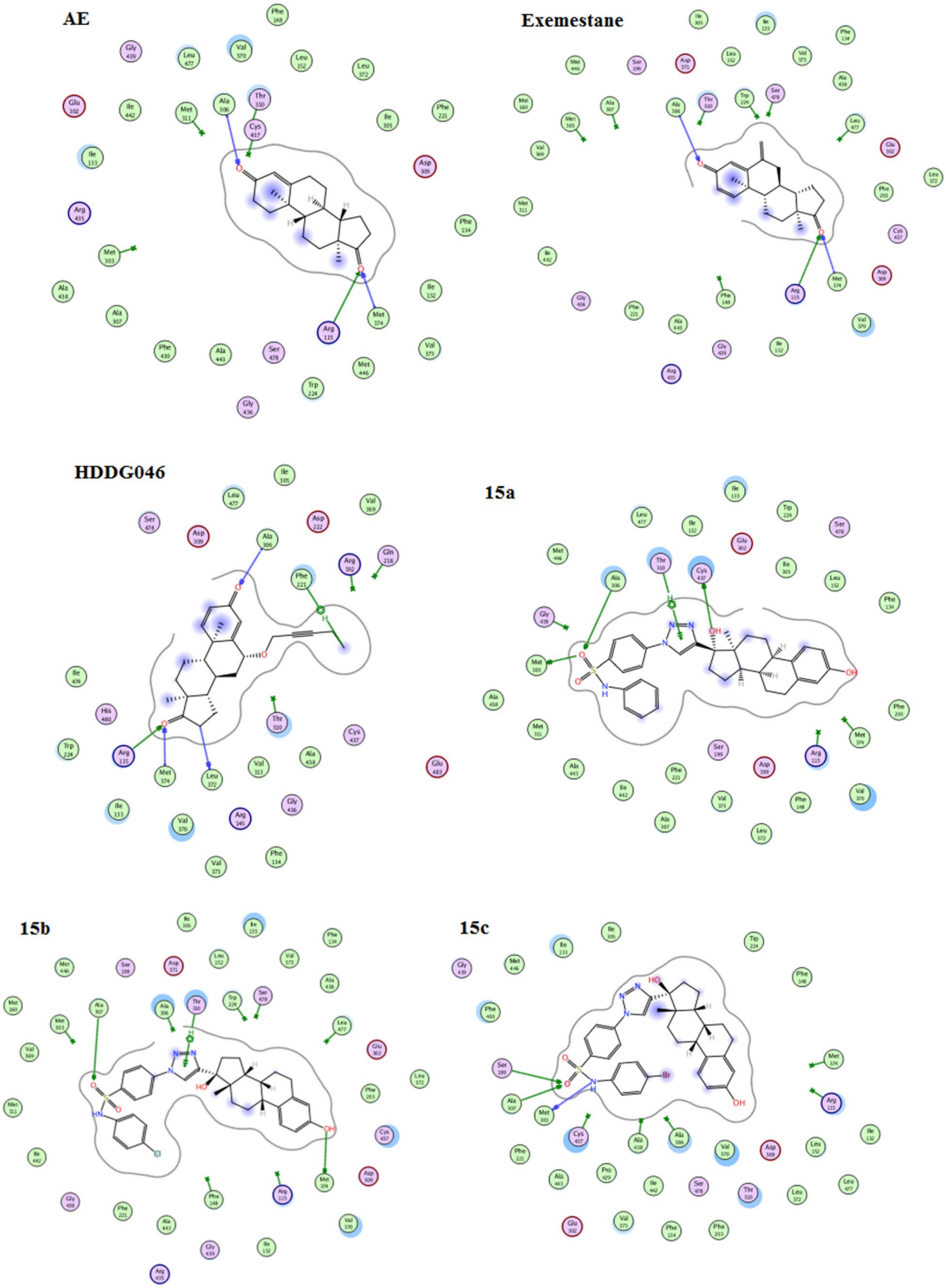


**Fig. 10** Binding of hybrids **15a**–**15f**, AE, exemestane, and HDDG046 into the active site of pAROM (5JL9) as assessed by MOE software

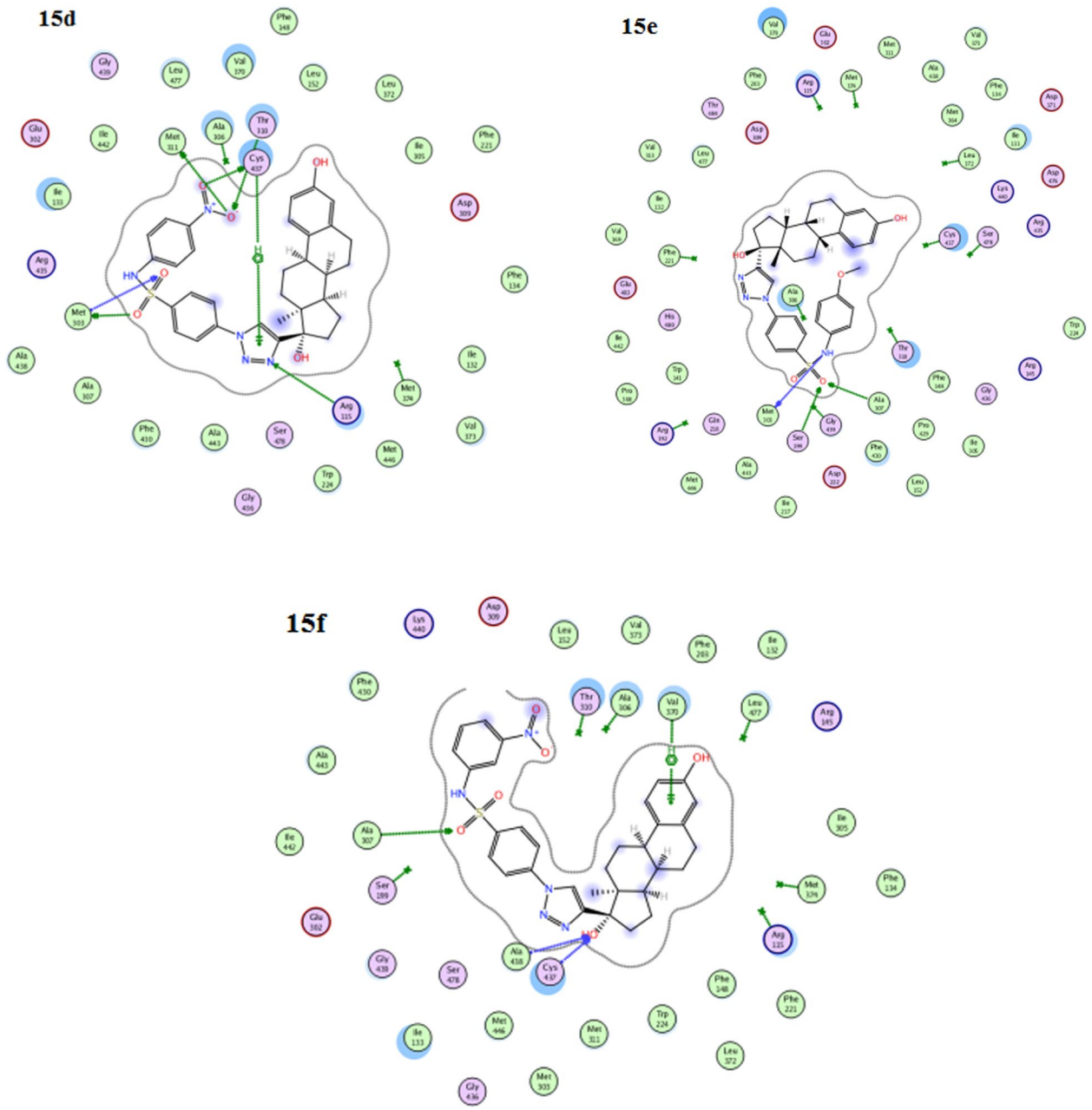


**Fig. 10** (continued)

Stirring was continued at room temperature for 16 h, then pyridine was removed azeotropically with toluene under vacuum, followed by dissolving the residue in EtOAc ($2 \times 5$ cm$^3$), collected extracts were dried with $Na_2SO_4$, and finally concentrated under vacuum to afford corresponding sulfonamide derivatives **14a**–**14f**. Physical properties agree with those already published [30].

## General procedure for preparation of hybrids 15a–15f

To a solution of ethinyl estradiol (EE, 0.67 mmol) in a mixture of THF/$H_2O$ (12 cm$^3$; 2:1), **14a**–**14f** (0.67 mmol), $CuSO_4$ (0.06 mmol), and sodium ascorbate (0.12 mmol) were added. The resulting mixture was stirred at room

temperature for 20–24 h, and the residue was extracted with $CH_2Cl_2$ (3 × 10 $cm^3$). The organic layer was washed twice with water, brine, and dried over anhydrous $Na_2SO_4$.

**4-[4-(17*α*-1,3,5(10)-Estratrien-3,17*β*-diol)-1*H*-1,2,3-triazol-1-yl]-*N*-phenylbenzenesulfonamide (15a, $C_{32}H_{34}N_4O_4S$)** Purification was achieved using flash chromatography (ethyl acetate/hexane, 1:3) which provided white solid (88%) **15a**. M.p.: 212–214 °C; $^1$H NMR (DMSO-$d_6$, 500 MHz): $\delta$ = 10.40 (brs, 1H, –$NHSO_2$–), 8.96 (brs, 1H, ArOH), 8.65 (s, 1H, triazole = CH), 8.11 (d, *J* = 9 Hz, 2H, ArH), 7.91 (d, *J* = 9 Hz, 2H, ArH), 7.21 (t, *J* = 8 Hz, 2H, ArH), 7.07 (d, *J* = 7.5 Hz, 2H, ArH), 7.01 (t, *J* = 7 Hz, 1H, ArH), 6.91 (d, *J* = 8.5 Hz, 1H, H-1), 6.44 (dd, *J* = 2.5 Hz, 8.5 Hz, 1H, H-2), 6.39 (d, *J* = 2.5 Hz, 1H, H-4), 5.31 (s, 1H), 2.67 (m, 2H, H-6), 2.38 (m, 1H), 2.10–1.98 (m, 2H), 1.84–1.78 (m, 3H), 1.63–1.61 (m, 1H), 1.54–1.45 (m, 2H), 1.35–1.1.20 (m, 3H), 1.06–1.01 (m, 1H), 0.94 (s, 3H, $CH_3$, H-18) ppm; $^{13}$C NMR (DMSO-$d_6$, 125 MHz): $\delta$ = 155.8 (C-3), 154.8, 139.3, 139, 137.1, 130.4, 129.2 (2 CHAr), 128.6 (2 CHAr), 125.9, 120.9, 120.5 (2 CHAr), 120 (2 CHAr), 116.7, 114.9, 112.7, 81 (C-17), 47.7, 46.8, 43.1, 37.3, 32.7, 29.2, 27.1, 26.0, 21.8, 18.3, 14.3 ($CH_3$, C-18) ppm; HRMS (ESI+): *m/z* calcd. for $C_{32}H_{34}N_4O_4S$ ([M + H]$^+$) 570.2301, found 570.2309.

**4-[4-(17*α*-1,3,5(10)-Estratrien-3,17*β*-diol)-1*H*-1,2,3-triazol-1-yl]-*N*-(4-chlorophenyl)benzenesulfonamide (15b, $C_{32}H_{33}ClN_4O_4S$)** Purification was achieved using flash chromatography (ethyl acetate/hexane, 1:3) which provided white solid (77%) **15b**. M.p.: 203–205 °C; $^1$H NMR (DMSO-$d_6$, 500 MHz): $\delta$ = 10.55 (brs, 1H, –$NHSO_2$–), 9.00 (brs, 1H, ArOH), 8.61 (s, 1H, triazole = CH), 8.07 (d, *J* = 9 Hz, 2H, ArH), 7.88 (d, *J* = 9 Hz, 2H, ArH), 7.24 (t, *J* = 5 Hz, 2H, ArH), 7.04 (t, *J* = 8.5 Hz, 2H, ArH), 6.91 (d, *J* = 8 Hz, 1H, H-1), 6.44–6.39 (m, 2H, H-2, H-4), 5.34 (s, 1H), 2.66 (m, 2H, H-6), 2.38 (m, 1H), 2.15–1.77 (m, 5H), 1.62–1.20 (m, 7H), 1.05–1.03 (m, 1H), 0.93 (s, 3H, $CH_3$, H-18) ppm; $^{13}$C NMR (DMSO-$d_6$, 125 MHz): $\delta$ = 155.8 (C-3), 154.9, 139.7, 137.2, 131.6, 130.5, 129.0 (2 CHAr), 128.6 (2 CHAr), 126.1, 122.1 (2 CHAr), 121.0, 120.1 (2 CHAr), 116.7, 114.9, 112.7, 81.1 (C-17), 47.8, 46.9, 43.1, 37.8, 32.8, 29.3, 27.2, 26.1, 23.6, 20.3, 17.8, 14.4 ($CH_3$, C-18) ppm; HRMS (ESI+): *m/z* calcd. for $C_{32}H_{33}ClN_4O_4S$ ([M + H]$^+$) 604.1911, found 604.2001.

**4-[4-(17*α*-1,3,5(10)-Estratrien-3,17*β*-diol)-1*H*-1,2,3-triazol-1-yl]-*N*-(4-bromophenyl)benzenesulfonamide (15c, $C_{32}H_{33}BrN_4O_4S$)** Purification was achieved using flash chromatography (ethyl acetate/hexane, 1:3) which provided white solid (91%) **15c**. M.p.: 225–226 °C; $^1$H NMR (DMSO-$d_6$, 500 MHz): $\delta$ = 10.56 (br s, 1H, –$NHSO_2$–), 8.98 (br s, 1H, ArOH), 8.64 (s, 1H, triazole = CH), 8.13 (app. d, *J* = 9 Hz, 2H, ArH), 7.92 (app. d, *J* = 7 Hz, 2H, ArH), 7.42 (app. d, *J* = 9 Hz, 2H, ArH), 7.06 (app. d, *J* = 6.5 Hz, 2H, ArH), 6.91 (d, *J* = 8.5 Hz, 1H, H-1), 6.44 (dd, *J* = 3 Hz, 8.5 Hz, 1H, H-2), 6.39 (d, *J* = 3 Hz, 1H, H-4), 5.34 (s, 1H), 2.67–2.63 (m, 2H, H-6), 2.38 (m, 1H), 2.10–1.98 (m, 2H), 1.84–1.78 (m, 3H), 1.62–1.20 (m, 6H), 1.05–1.03 (m, 1H), 0.94 (s, 3H, $CH_3$, H-18) ppm; $^{13}$C NMR (DMSO-$d_6$, 125 MHz): $\delta$ = 155.9 (C-3), 154.9, 139.7, 138.6, 137.2, 136.8, 132.5 (2 CHAr), 130.5, 128.7 (2 CHAr), 126.5, 122.3 (2 CHAr), 121.0, 120.2 (2 CHAr), 116.7, 114.9, 112.7, 81.1 (C-17), 47.8, 46.9, 43.1, 37.3, 32.8, 29.3, 27.2, 26.1, 23.6, 18.6, 14.4 ($CH_3$, C-18) ppm; HRMS (ESI+): *m/z* calcd. for $C_{32}H_{33}BrN_4O_4S$ ([M + H]$^+$) 648.1406, found 648.1413.

**4-[4-(17*α*-1,3,5(10)-Estratrien-3,17*β*-diol)-1*H*-1,2,3-triazol-1-yl]-*N*-(4-nitrophenyl)benzenesulfonamide (15d, $C_{32}H_{33}N_5O_6S$)** Purification was achieved using flash chromatography (ethyl acetate/hexane, 1:3) which provided white solid (73%) **15d**. M.p.: 223–224 °C; $^1$H NMR (DMSO-$d_6$, 500 MHz): $\delta$ = 11.4 (s, 1H, –$NHSO_2$–), 8.98 (brs, 1H, ArOH), 8.65 (s, 1H, triazole = CH), 8.14 (dd, *J* = 9 Hz, 9 Hz, 4H, ArH), 8.05 (d, *J* = 8.5 Hz, 2H, ArH), 7.31 (d, *J* = 9.5 Hz, 2H, ArH), 6.90 (d, *J* = 8.5 Hz, 1H, H-1), 6.44–6.38 (m, 2H, H-2, H-4), 5.34 (s, 1H), 2.67 (m, 2H, H-6), 2.40–2.25 (m, 2H), 2.10–1.78 (m, 4H), 1.63–1.12 (m, 7H), 1.08–0.93 (m, 4H) ppm; $^{13}$C NMR (DMSO-$d_6$, 125 MHz): $\delta$ = 167.1 (C–$NO_2$), 155.9 (C-3), 139.9, 137.2, 132.0, 130.4, 128.8 (2 CHAr), 126.0, 125.5 (2 CHAr), 121.1, 120.4 (2 CHAr), 118.3 (2 CHAr), 116.4, 114.9, 112.7, 81.1 (C-17), 47.8, 46.9, 43.1, 37.3, 32.2, 29.3, 27.4, 23.3, 22.4, 18.6, 14.4 ($CH_3$, C-18) ppm; HRMS (ESI+): *m/z* calcd. for $C_{32}H_{33}N_5O_6S$ ([M + H]$^+$) 615.2152, found 615.2155.

**4-[4-(17*α*-1,3,5(10)-Estratrien-3,17*β*-diol)-1*H*-1,2,3-triazol-1-yl]-*N*-(4-methoxyphenyl)benzenesulfonamide (15e, $C_{33}H_{36}N_4O_5S$)** Purification was achieved using flash chromatography (ethyl acetate/hexane, 1:3) which provided white solid (68%) **15e**. M.p.: 178–180 °C; $^1$H NMR (DMSO-$d_6$, 500 MHz): $\delta$ = 10.01 (s, 1H, –$NHSO_2$–), 8.97 (brs, 1H, ArOH), 8.66 (s, 1H, triazole = CH), 8.11 (t, *J* = 7 Hz, 2H, ArH), 7.82 (d, *J* = 9 Hz, 2H, ArH), 7.72 (dd, *J* = 9 Hz, 1.5 Hz, 2H, ArH), 6.90 (dd, *J* = 2.5 Hz, 7.0 Hz, 2H, ArH), 6.80 (dd, *J* = 1.5 Hz, 9 Hz, 1H, H-1), 6.45–6.39 (m, 2H, H-2, H-4), 5.32 (s, 1H), 3.66 (s, 3H, $OCH_3$), 2.67 (m, 2H, H-6), 2.40–2.25 (m, 2H), 2.10–1.75 (m, 5H), 1.62–1.15 (m, 7H), 0.94 (s, 3H, $CH_3$, H-18) ppm; $^{13}$C NMR (DMSO-$d_6$, 125 MHz): $\delta$ = 156.8 (C-3), 154.9, 144.6, 139.3, 138.6, 137.1, 136.1, 128.9, 128.6, 126.5, 124.0 (4 CHAr), 116.8, 114.9, 114.3 (4 CHAr), 112.7, 81.1 (C-17), 56.1 ($OCH_3$), 47.8, 46.9, 43.1, 37.5, 32.4, 29.1, 27.3, 26.1, 22.4, 18.1, 13.9 ($CH_3$, C-18) ppm; HRMS (ESI+): *m/z* calcd. for $C_{33}H_{36}N_4O_5S$ ([M + H]$^+$) 600.2406, found 600.2415.

**4-[4-(17*α*-1,3,5(10)-Estratrien-3,17*β*-diol)-1*H*-1,2,3-triazol-1-yl]-*N*-(3-nitrophenyl)benzenesulfonamide (15f, $C_{32}H_{33}N_5O_6S$)** Purification was achieved using flash chromatography (ethyl acetate/hexane, 1:3) which provided white solid (64%) **15f**. M.p.: 231–232 °C; $^1$H NMR (DMSO-$d_6$, 500 MHz): $\delta = 11.20$ (brs, 1H,–NHSO–), 8.96 (brs, 1H, ArOH), 8.65 (s, 1H, triazole = CH), 8.15 (d, $J = 9$ Hz, 2H, ArH), 7.95 (dd, $J = 8.5$ Hz, 8.5 Hz, 3H, ArH), 7.88 (m, 1H, ArH), 7.68 (m, 1H, ArH), 7.53 (m, 1H, ArH), 6.91 (m, 1H, H-1), 6.45–6.39 (m, 2H, H-2, H-4), 5.33 (s, 1H), 2.67 (m, 2H, H-6), 2.38 (m, 1H), 2.10–1.78 (m, 5H), 1.63–1.40 (m, 3H), 1.36–1.15 (m, 5H), 1.02 (m, 1H), 0.93 (s, 3H, $CH_3$, H-18) ppm; $^{13}$C NMR (DMSO-$d_6$, 125 MHz): $\delta = 165.9$ (C–$NO_2$), 154.9 (C-3), 139.8, 137.2, 130.9, 130.4, 128.7 (2 CHAr), 125.7, 125.5, 121.1, 120.4 (2 CHAr), 116.8, 114.9, 113.7, 112.7, 81.1 (C-17), 47.8, 46.9, 43.1, 37.8, 32.3, 29.3, 27.2, 25.5, 22.8, 18.6, 14.4 ($CH_3$, C-18) ppm; HRMS (ESI+): *m/z* calcd. for $C_{32}H_{33}N_5O_6S$ ($[M + H]^+$) 615.2152, found 615.2158.

## Cytotoxic studies

### Cell cultures and MTT cytotoxic assays

The pure cultures breast cancer cell line (MCF-7; ATCC® HTB-22) was obtained from American Type Culture Collection (ATCC®). Normal fibroblast cells (F180) were obtained from VACSERA-Egypt. Cell viability was assessed by MTT assay as described elsewhere [18].

### Cell cycle analysis and assessment of apoptosis

The apoptotic effect of synthesized hybrids **15a**–**15f** was analyzed by propidium iodide (PI) flow cytometry kit for cell cycle analysis (Annexin V Apoptosis Detection Kit®) according to the manufacturer's instructions. Data analysis and nuclear morphology of apoptotic cells were examined using BD FACS Calibur. Propidium iodide histograms of normal and treated cells with the cell count on the *y*-axis and the propidium iodide fluorescence intensity on the *x*-axis were recorded. In addition, the cell cycle arrest caused by hybrids **15a**–**15f** in a concentration-dependent manner in MCF-7 cells was examined.

### Aromatase enzyme inhibition assay

The assay was carried out using the Gentest kit (BioVision®, catalog # K893-100) using the CYP19A (human microsomal and S9 fractions; EC 1.14.14.14; K983-100-1) enzyme and *O*-benzylfluorescein benzyl ester (DBF; K983-100-2) as a fluorimetric substrate according to manufacturer's instructions. Briefly, in a 96-well black plate, a mixture of 0.1 $cm^3$ the cofactor (0.08 $cm^3$ of 50 mM phosphate buffer, pH 7.4; 0.02 $cm^3$ of 20 × NADPH-generating system, 26 mM $NADP^+$, 66 mM glucose-6-phosphate, and 66 mM $MgCl_2$); and 0.001 $cm^3$ of 100 μ/$cm^3$ glucose-6-phosphate dehydrogenase, were added and incubated at 37 °C for 10 min. The reaction was initiated by adding 0.1 $cm^3$ of enzyme/substrate mixture (0.8 $cm^3$ of 50 mM phosphate buffer, pH 7.4; 0.12 $cm^3$ of 16 pmol/$cm^3$ CYP19; $2 \times 10^{-3}$ $cm^3$ of 0.2 mM DBF) and 0.01 $cm^3$ of each concentration (10,000, 1000, 100, 10, and 0 ng/$cm^3$) of test hybrids **15a**–**15f**, negative control (10% DMSO), or letrozole (K983-100-3) as positive control. Fluorescence was recorded at $\lambda_{max} = 488/527$ nm with cut-off 515 nm. Percentage (%) inhibition was calculated using the following equation: % inhibition = 100 − [(sample − blank)/(DMSO − blank) × 100].

## Molecular modelling studies

Molecular modeling and visualization processes were performed within the aromatase active site using Molecular Operating Environment (MOE: 2014.09) software (Chemical Computing Group, Montreal, QC, Canada). The co-crystal structure was retrieved from the RCSB Protein Data Bank (PDB code 3EQM). First, the compounds (AE, exemestane, HDDG046, and hybrids **15a**–**15f**) were prepared with the standard protocol designated in the MOE program. However, the energy of the docked structures was minimized using MMF94FX forcefield with gradient RMS of 0.01 kcal/mol, then the protein structure was prepared using the MOE LigX protocol. To validate the docking study at the aromatase active site, the native ligand androstenedione was re-docked into the binding site using the same set of parameters as described above. The ligands were then docked into the binding site using the triangle matcher placement method. Refinement was carried out using Forcefield and scored using the Affinity δG scoring system. The resulting docking poses were visually inspected, and the pose of the lowest binding free energy value was considered.

**Acknowledgements** Special thanks to Prof. Gamal Abu-Rahmah, Department of Pharmaceutical Chemistry, Faculty of Pharmacy, Minia University for his advises through the research work, also to Dr. Abu-Baker Mostafa, Department of Pharmaceutical Organic Chemistry, Faculty of Pharmacy, Assiut University for his guidance through chemistry part, and finally, for Dr. A. Y. Desoky, Department of Chemistry, Faculty of Science, the University of Waterloo for running mass spectral analysis for our group.

## References

1. Hu W, Huang XS, Wu JF, Yang L, Zheng YT, Shen YM, Li ZY, Li X (2018) J Med Chem 61:8947
2. Erşatır M, Yıldırım M, Giray ES, Yalın S (2020) Monatsh Chem 151:625

3. Vaidya A, Jain S, Prashantha Kumar B, Singh SK, Kashaw SK, Agrawal RK (2020) Monatsh Chem 151:385
4. Li Z, Chen Y, Liu Z, Wang Q, Zhao Y, Wei J, Liu M, Wang Z, Li D, Han J (2020) Monatsh Chem 151:353
5. Acar Cevik U, Saglik BN, Osmaniye D, Levent S, Kaya Cavusoglu B, Karaduman AB, Ozkay Y, Kaplancikli ZA (2020) Arch Pharm 353(5):e2000008
6. Chia S, Gradishar W, Mauriac L, Bines J, Amant F, Federico M, Fein L, Romieu G, Buzdar A, Robertson JF, Brufsky A, Possinger K, Rennie P, Sapunar F, Lowe E, Piccart M (2008) J Clin Oncol 26:1664
7. Miller WR, Bartlett JM, Canney P, Verrill M (2007) Breast Cancer Res Treat 103:149
8. Ghosh D, Griswold J, Erman M, Pangborn W (2010) J Steroid Biochem Mol Biol 118:197
9. Favia AD, Nicolotti O, Stefanachi A, Leonetti F, Carotti A (2013) Expert Opin Drug Discov 8:395
10. Macedo LF, Sabnis G, Brodie A (2009) Ann N Y Acad Sci 1155:162
11. Santen RJ, Brodie H, Simpson ER, Siiteri PK, Brodie A (2009) Endocr Rev 30:343
12. Espinoza-Fonseca LM (2006) Bioorg Med Chem 14:896
13. Mencher SK, Wang LG (2005) BMC Clin Pharmacol 5:3
14. Morphy R, Kay C, Rankovic Z (2004) Drug Discov Today 9:641
15. Gediya LK, Njar VC (2009) Expert Opin Drug Discov 4:1099
16. Viegas-Junior CDA, da Silva BV, Barreiro EJ, Fraga CAM (2007) Curr Med Chem 14:1829
17. Meegan NMO, Ba MJ (2011) Curr Med Chem 18:4722
18. El-Sheref EM, Aly AA, Ameen MA, Brown AB (2019) Monatsh Chem 150:747
19. Mahdavi M, Saeedi M, Karimi M, Foroughi N, Hasanshahi F, Alinezhad H, Foroumadi A, Shafiee A, Akbarzadeh T (2016) Monatsh Chem 147:2151
20. Doiron J, Soultan AH, Richard R, Toure MM, Picot N, Richard R, Cuperlovic-Culf M, Robichaud GA, Touaibia M (2011) Eur J Med Chem 46:4010
21. Pingaew R, Mandi P, Nantasenamat C, Prachayasittikul S, Ruchirawat S, Prachayasittikul V (2014) Eur J Med Chem 81:192
22. Pingaew R, Prachayasittikul V, Mandi P, Nantasenamat C, Prachayasittikul S, Ruchirawat S, Prachayasittikul V (2015) Bioorg Med Chem 23:3472
23. Pingaew R, Mandi P, Prachayasittikul V, Prachayasittikul S, Ruchirawat S, Prachayasittikul V (2018) Eur J Med Chem 143:1604
24. Ghorab MM, Alsaid MS, Al-Ansary GH, Abdel-Latif GA, Abou El Ella DA (2016) Eur J Med Chem 124:946
25. Ghorab MM, Alsaid MS, Samir N, Abdel-Latif GA, Soliman AM, Ragab FA, Abou El Ella DA (2017) Eur J Med Chem 134:304
26. Ghosh D, Lo J, Morton D, Valette D, Xi J, Griswold J, Hubbell S, Egbuta C, Jiang W, An J, Davies HM (2012) J Med Chem 55:8464
27. Ziemer B, Sauer E (1998) Acta Crystallogr Sect C Cryst Struct Commun 54:IUC9700034
28. Ueno T, Toriumi M, Nonogaki S, Hashimoto M, Hayashi N, Tadano K, Iwayanagi T (1990) Azidobenzenesulfonates, their preparation, and their use in photosensitive materials for photolithographic imaging. Patent DE 3941757, Jun 21, 1990; (1991) Chem Abstr 114:52928
29. Mirian M, Zarghi A, Sadeghi S, Tabaraki P, Tavallaee M, Dadrass O, Sadeghi-Aliabadi H (2011) Iran J Pharm Res 10:741
30. El-Kardocy A, Mustafa M, Ahmed ER, Mohamady S, Mostafa YA (2019) Med Chem Res 28:2088
31. Woo LW, Bubert C, Purohit A, Potter BV (2011) ACS Med Chem Lett 2:243
32. Kalder M, Hadji P (2014) Breast Care 9:312
33. Chan KT, Meng FY, Li Q, Ho CY, Lam TS, To Y, Lee WH, Li M, Chu KH, Toh M (2010) Cancer Lett 294:118
34. Ghosh D, Egbuta C, Lo J (2018) J Steroid Biochem Mol Biol 181:11